Supplementary Information

Understanding the Ag-S Interface Stability and Electrocatalytic Activity of CO_2 Electroreduction in Atomically Precise Ag_{25} Nanoclusters

Yuting Ye,[a,⊥] Xia Zhou,[b,⊥] Yuping Chen,[a] Likai Wang*[b] and Qing Tang*[a]

a School of Chemistry and Chemical Engineering, Chongqing Key Laboratory of Chemical Theory and Mechanism, Chongqing University, Chongqing 401331, China

E-mail: qingtang@cqu.edu.cn

b School of Chemistry and Chemical Engineering, Shandong University of Technology, Zibo, Shandong, 255049, China

E-mail: lkwangchem@sdut.edu.cn

[⊥] These two authors contributed equally to this work.

DFT Method Details. All molecular dynamics simulations and constrained AIMD simulations were performed by employing the CP2K/Quickstep package.[1, 2] The method uses an atom-centered Gaussian-type basis set to describe the wave function, but an auxiliary plane wave basis set was employed to describe the density. Representing the density in terms of plane waves or a regular grid allows the efficiency of the Fast Fourier Transform (FFT) to be exploited to solve the Poisson equation and to obtain the Hartree energy in a time that scales linearly with the size of the system.[2] The electronic structure calculations are described by DFT with the spin-polarized Perdew−Burke−Ernzerhof (PBE) functional and mixed double-ζ Gaussian and plane-wave (GPW) basis sets with an energy cutoff of 400 Ry.[3] The core electrons were modeled by Goedecker-Teter-Hutter (GTH) for the pseudopotentials of Ag, S, C, Na, F O, and H, respectively.[1] The MD simulations were sampled by the canonical (NVT) ensemble employing Nose−Hoover thermostats with a time step of 1.0 fs at the target

temperature of 300 K. [4, 5] We conducted constrained DFT-MD simulations to evaluate the kinetic free energy barriers associated with the process of thiolate leaching, carbon dioxide electroreduction(CO_2RR) and hydrogen evolution reaction (HER) under neutral conditions. During these simulations, the kinetic potential is determined by imposing an overall constraint on the reaction coordinate variables (CV, ζ), the energy barriers are determined by a computational simulation of approximately 3-5 ps set relative to the CV value.[1] We set the growth rate of the CV ($d\zeta$) to 0.0005, which was determined to be the optimal value for driving the chemical reaction.

Potential Calculations. The applied potential was calculated according to $U_{RHE} = (\Phi - 4.44)/e + 0.0592 \times pH$.[6] The work function Φ of each state is derived by averaging 5 snapshots from the AIMD trajectories.

Free Energy Calculations. The kinetic barriers are obtained by applying a holonomic constraint on the reaction coordinate (ζ) during constrainted DFT-MD simulations.

For H adsorption on the S site, the distance between S and H atoms is chosen as the collective variable (CV), which is defined by eq 1:

$$CV = \zeta(r) = |r_{OH} - r_{SH}| \tag{1}$$

where r_{OH} refer to the coordinates of the O atom of H_2O and the H atom of H_2O, and r_{SH} refer to the coordinates of the S atom of M_{25} (M=Au, Ag) and the H atom of H_2O.

For $-SCH_3$ ligand removal from the metal site, the CV is defined by eq 2:

$$CV = \zeta(r) = |r_M + r_S| \tag{2}$$

where r_M refer to the coordinates of the Au/Ag atom and r_S refer to the coordinates of the S atom of M_{25} (M=Au, Ag).

For CO_2 adsorption on the metal site ($CO_2 + e^- + * \rightarrow *CO_2^-$), the CV is defined by eq 3：

$$CV = \zeta(r) = |r_M - r_C| \tag{3}$$

where * represent the active site, r_M and r_C refer to the coordinates of the metal atom and the C atom of CO_2.[1]

Chemicals and materials. Silver nitrate ($AgNO_3$, AR), Tetrachloroauric (III) acid ($HAuCl_4 \cdot 3H_2O$, >99.99%), tetraoctylammonium bromide (TOAB, 98%), 2-

Phenylethylmercaptan (PET, 98%), 2,4-dimethylbenzenethiol (HSPhMe$_2$, 95%), tetraphenylphosphonium bromide (PPh$_4$Br, 98%), sodium borohydride (NaBH$_4$) and potassium hydroxide (KOH, >85%), Nafion solution (5 wt%), tetrahydrofuran (THF), methanol, dichloromethane (CH$_2$Cl$_2$) and ethanol were used without further purification.

Preparation of Au$_{25}$(PET)$_{18}$ NCs. This method was based on the procedure outlined in the previous report.[7] Firstly, HAuCl$_4$•3H$_2$O (0.1mmol) and TOAB (0.12 mmol) were dissolved in THF (12 ml) in a 50 ml vial. After vigorous stirring for 15 mins, the solution color changed from orange to red. Then 0.32 mmol of PhCH$_2$CH$_2$SH was slowly added to the above solution and stirred continuously for 1 h until the red solution turned colorless. Secondly, a freshly prepared solution of NaBH$_4$ (1 mmol) in 2 mL cold water was quickly added to the above solution, causing it to turn black immediately, indicating the formation of gold clusters. After stirring for an additional 24 h, the product solution was transferred to a 25 mL round-bottom flask and dried using rotary evaporation. Finally, the product was washed with ethanol and collected by centrifugation to completely remove impurities. Additionally, the as-prepared Au$_{25}$(PET)$_{18}$ NCs were dissolved in CH$_2$Cl$_2$ and bubbled with O$_2$ for 20 min to fully convert them into charge neutral Au$_{25}$(PET)$_{18}$ NCs.

Preparation of Ag$_{25}$(SPhMe$_2$)$_{18}$ NCs. This procedure was similar to the previous report.[8] 38 mg of AgNO$_3$ (0.22 mmol) was dissolved in 2 mL of methanol in a 25 mL glass vial with the sonication, and 90 μL of HSPhMe$_2$ (0.66 mmol) was then added, yielding a thick yellow mixture. Afterward, 18 mL of CH$_2$Cl$_2$ was added, and the solution was stirred for 20 mins in an ice bath. A freshly prepared solution of PPh$_4$Br (7 mg, 0.016 mmol) in methanol (0.5 mL) was then added into the above solution, subsequently 0.5 mL of ice-cold aqueous NaBH$_4$ (15 mg, 0.4 mmol) solution was drop-wise added. And the color of the reaction mixture turned from light yellow to dark. After stirring of 6 h, the top water layer was pipetted off, and the solution was dried and washed with methanol several times to achieve the product.

Electrochemical measurements. The catalytic activity of Au$_{25}$ and Ag$_{25}$ NCs were obtained using an electrochemical workstation (CHI 760E) with a three-electrode

system coupled to a CO_2 flow cell. The electrolyte solution was 1 M KOH, and the reference electrode was an Ag/AgCl electrode (immersed in saturated KCl solution), an anion-exchange membrane, and a platinum plate used as the ion mobility channel and counter electrode, respectively. The working electrode was prepared as follows: 1 mg carbon nanotube and 1 mg catalysts were dissolved in 0.5 mL of CH_2Cl_2 to achieve a uniform dispersion ink containing 10 µL of 5 wt% Nafion solution, 0.5 mL of the above solution was sprayed onto 1 cm^2 (GDL) with the loading mass of 2 mg/cm^2. The potential in this work is converted to reversible hydrogen electrode (RHE) potential according to the equation:

$$E(RHE) = E(Ag/AgCl) + 0.197V + 0.0591 \times pH$$

The cathodic electrolyte was continuously saturated with CO_2 for 30 min before electrochemical CO_2 reduction reaction. The cathodic and anodic reaction chambers were separated by anion exchange membrane in alkaline media. In the electrocatalytic reduction process, each electrolyte cell contained 30 mL of electrolyte, which was circulated by a peristaltic pump at 40 rpm from the flow chamber to the corresponding electrolyte cell. The gas products were analyzed quantitatively and qualitatively with the aid of a gas chromatograph (GC, Huaai 9560).

Faraday efficiency of gas products was calculated based on the following formula (FE):

$$FE = \frac{Q_i}{Q_{total}} = \frac{N_i \times Z \times F}{Q_{total}}$$

where Q_i the charge required to form the gaseous product, Q_{total} is the total charge during the reaction, N_i is the number of moles of the product detected by gas chromatography, Z is the number of electrons transferred during the formation of the product (2 for CO and H_2), and F is Faraday's constant (96485 C mol^{-1}).

Calculation of the turnover frequency (TOF) was as follow:

$$TOF(h^{-1}) = \frac{j_i/ZF}{m_i * \omega / M} \times 3600$$

where j_i is the partial current density of the corresponding gas product, Z is the number of transferred electrons formed by the product (2 for CO), F is the Faraday constant (96485 C mol^{-1}), m_i is the mass of the loading catalyst, ω is the relative mass fraction of Au and Ag in the catalyst, and M is the relative atomic mass of Au and Ag. Linear

sweep voltammetry (LSV) was conducted in a 1M KOH solution saturated with either N_2 or CO_2, using a scan rate of 50 mV s^{-1}.
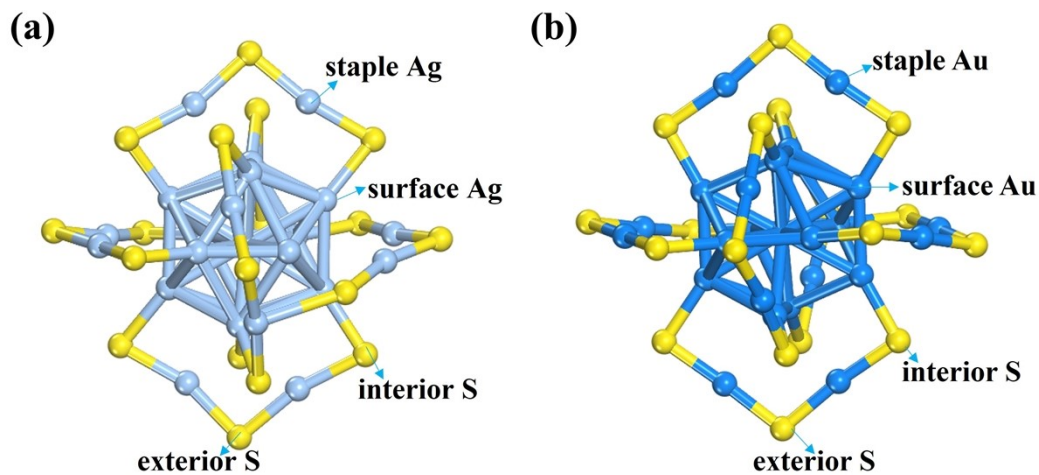

Fig.S1 Schematic Ag-S (Au-S) framework structure of (a) $Ag_{25}(SR)_{18}$ and (b) $Au_{25}(SR)_{18}$ nanoclusters. The pale blue, blue, and yellow colours indicate Ag, Au, and S atoms, respectively, and the R groups are omitted for clarity.
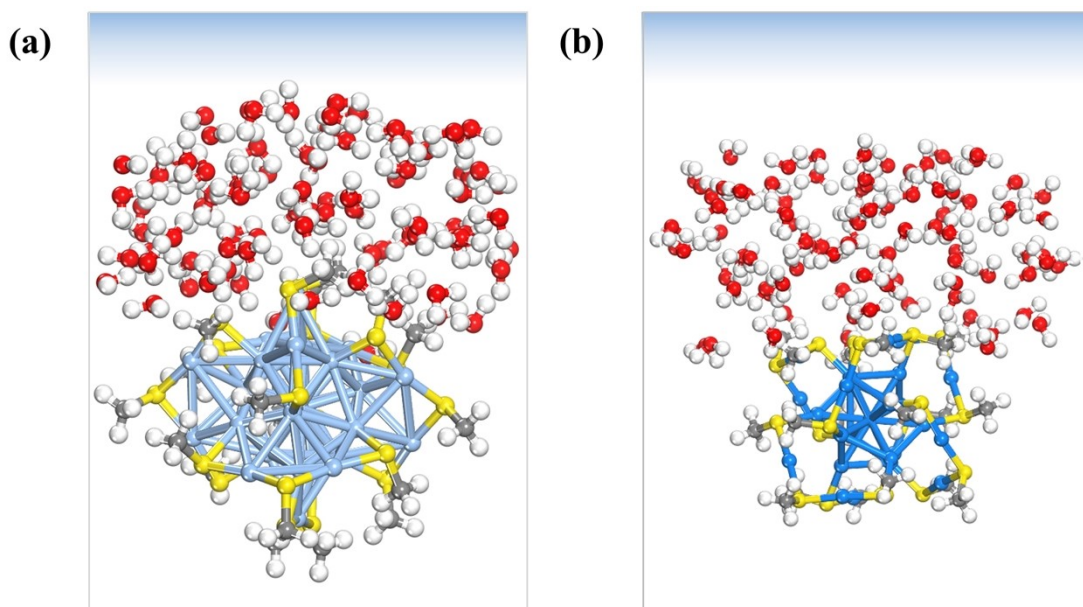

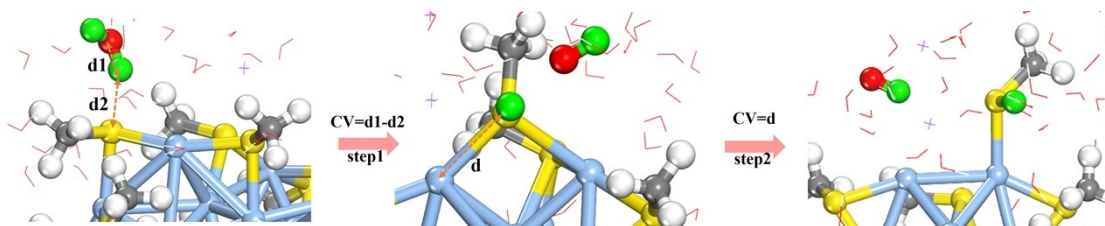Fig.S2 Side view of (a) $Ag_{25}(SCH_3)_{18}$/water model and (b) $Au_{25}(SCH_3)_{18}$/water model.

Fig.S3 Schematic local structures of *H adsorption to the S site and Ag-S bond breaking in $Ag_{25}(SCH_3)_{18}$. The defined collective variable (CV, d_1-d_2 or d) is shown inset. The H atoms from the attacked H_2O molecule are highlighted in green.
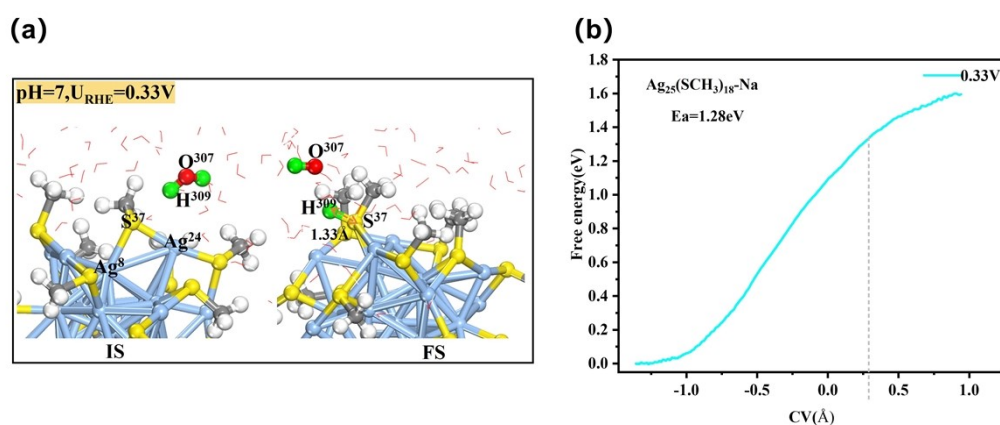
Fig.S4 (a) Schematic local structures (initial state, IS, and final state, FS) of *H adsorption to the S site of $Ag_{25}(SCH_3)_{18}$ at $U_{RHE} = 0.33V$. (b) Integral free energy curve for *H adsorption along the reaction coordinate.
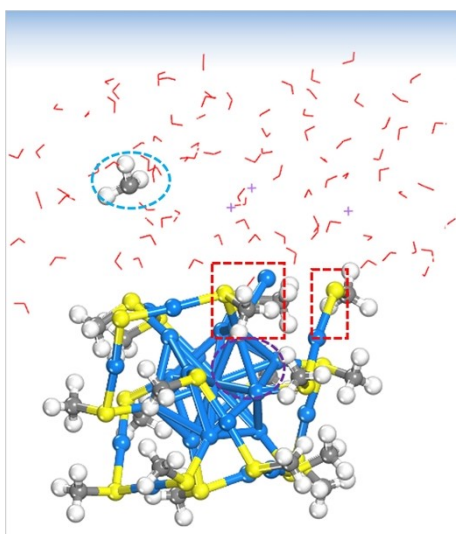
Fig. S5 Schematic representation of the Au_{25}/H_2O interface structure at $U_{RHE} = -1.30$ V in the neutral system.
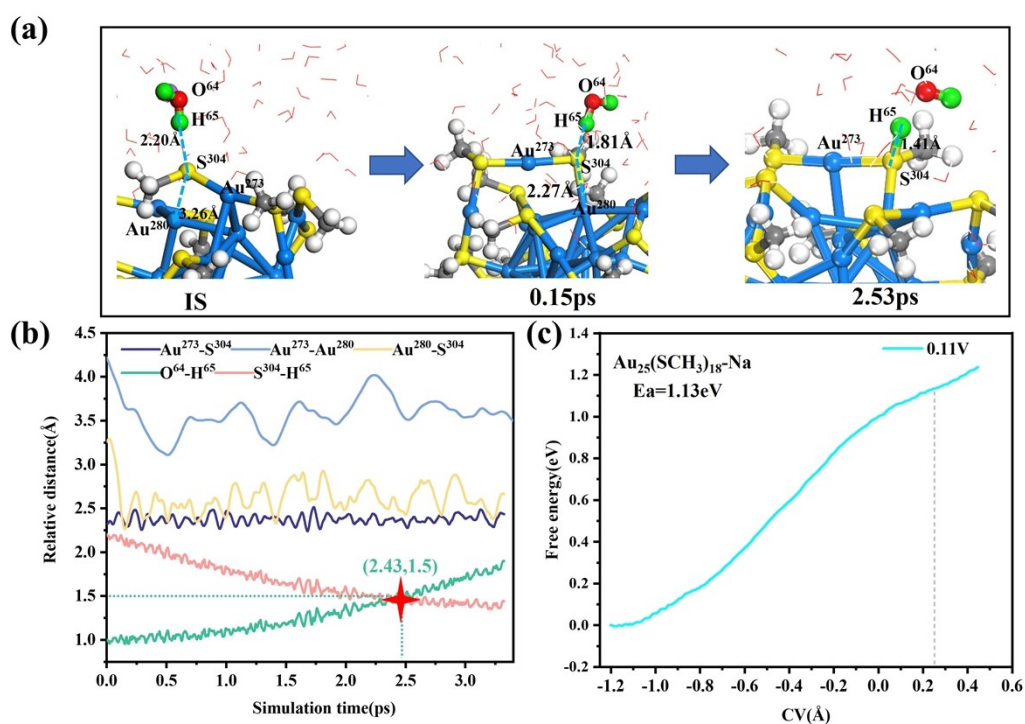
Fig.S6 (a) Schematic local structures of *H adsorption in $Au_{25}(SCH_3)_{18}$ at U_{RHE}=0.11V. Statistics of the relative distances between representative atoms (b) and the integral free energy curve (c) during constrained DFT-MD simulations at U_{RHE}=0.11V.
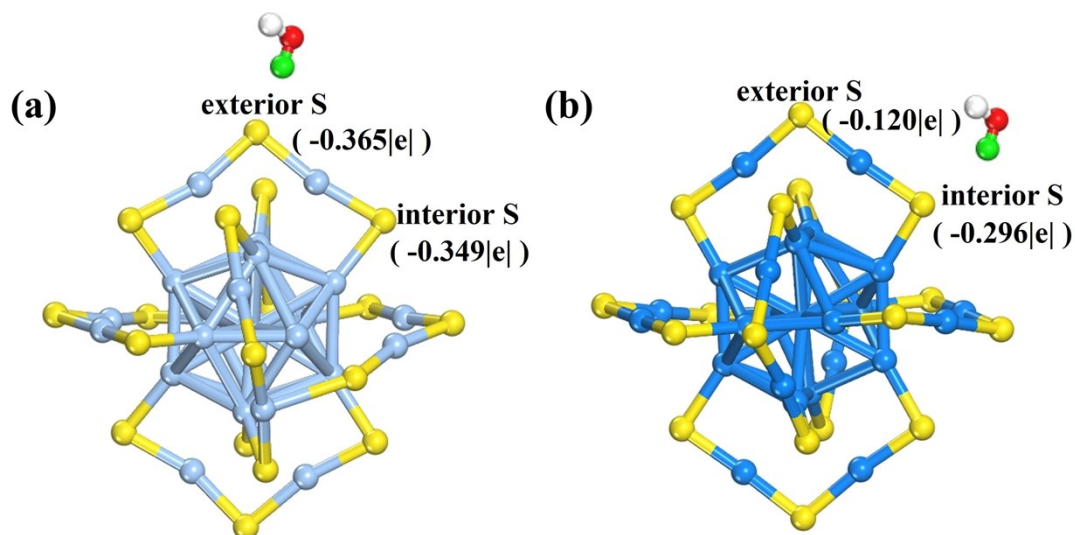

Fig.S7 The Bader charge of two different S sites in Ag_{25} (a) and Au_{25} (b) NCs at the cluster/water interface under electrochemical conditions.
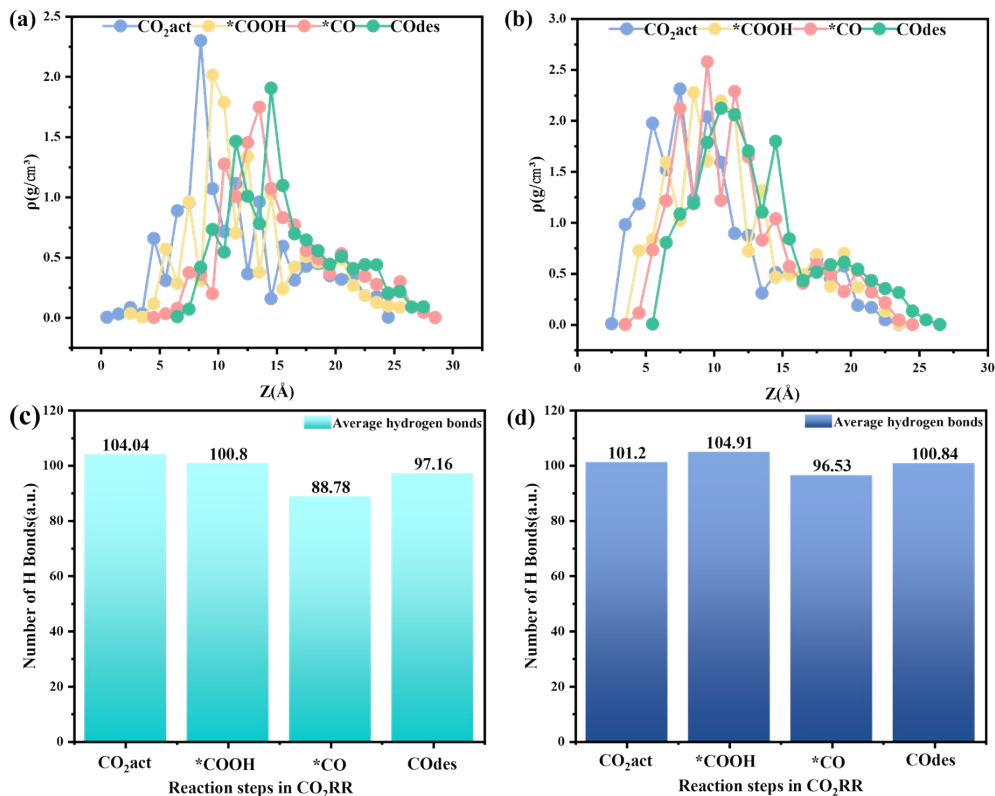
Fig.S8 Distribution of water density and the number of hydrogen bonds along the reaction coordinates for the Ag_{25}/water system (a, c) and the Au_{25}/water system (b, d) at different reaction steps of CO_2RR (*CO_2 activation, *COOH formation, *CO formation and CO desorption).
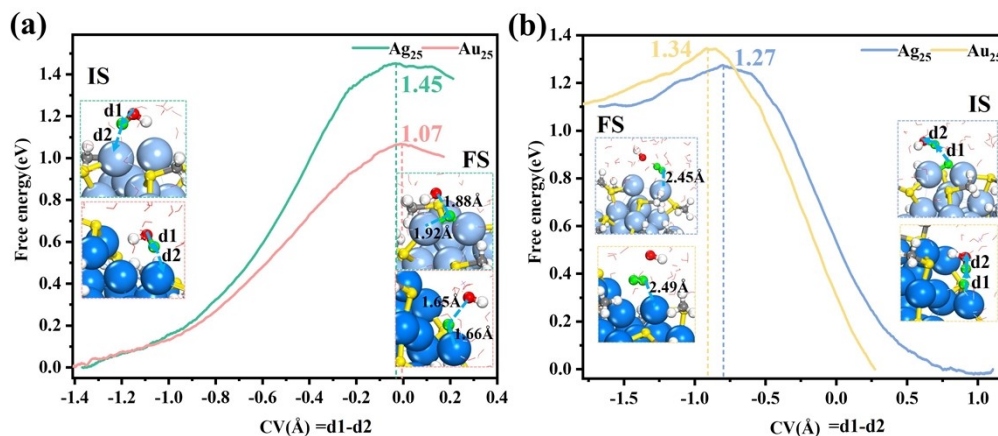

Fig.S9 Comparison of the integral free energy curves between Ag_{25} and Au_{25} in *H formation (a) and H_2 formation (b) of HER process. The local structures of initial state (IS), final state (FS) and the defined collective variable (CV, d_1-d_2) are shown inset.
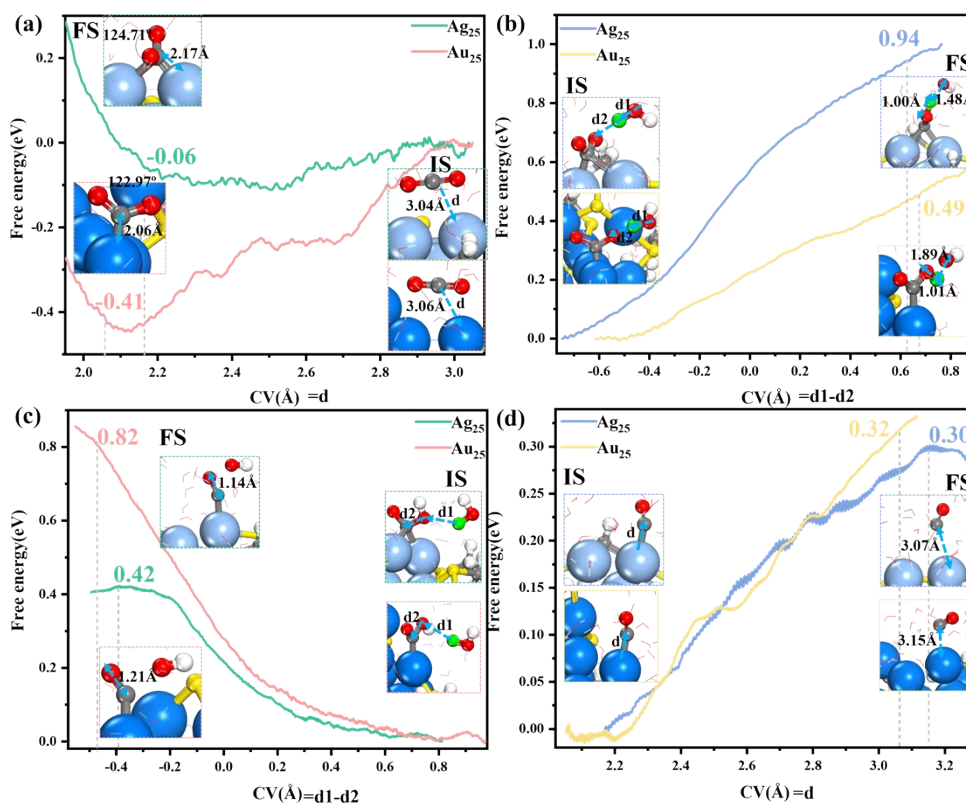
Fig.S10 Comparison of the integral free energy curves between Ag_{25} and Au_{25} protected by long-chain -SC_6H_{13} ligands in CO_2 activation (a), *COOH formation (b), *CO formation (c) and CO desorption (d) by constrained AIMD simulations. The local structures of initial state (IS), final state (FS) and the defined collective variable (CV, d_1-d_2 or d) are shown inset.
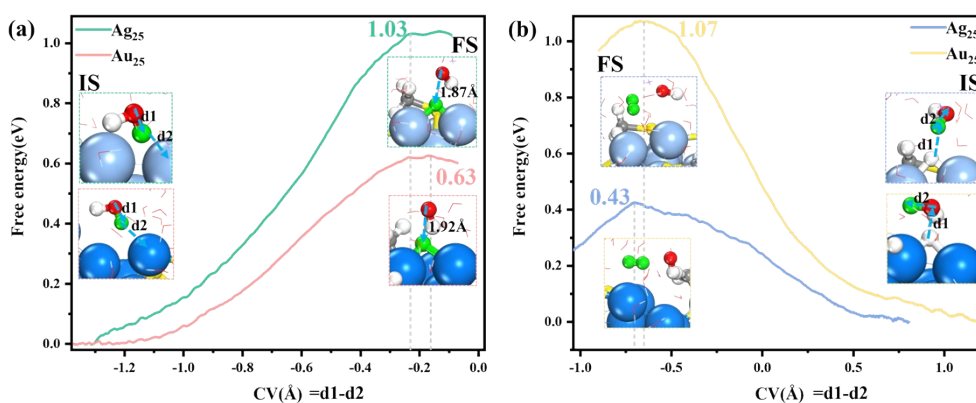

Fig.S11 Comparison of the integral free energy curves between Ag_{25} and Au_{25} protected by long-chain -SC_6H_{13} ligands in *H formation (a) and H_2 formation (b) of HER process. The local structures of initial state (IS), final state (FS) and the defined collective variable (CV, d_1-d_2) are shown inset.
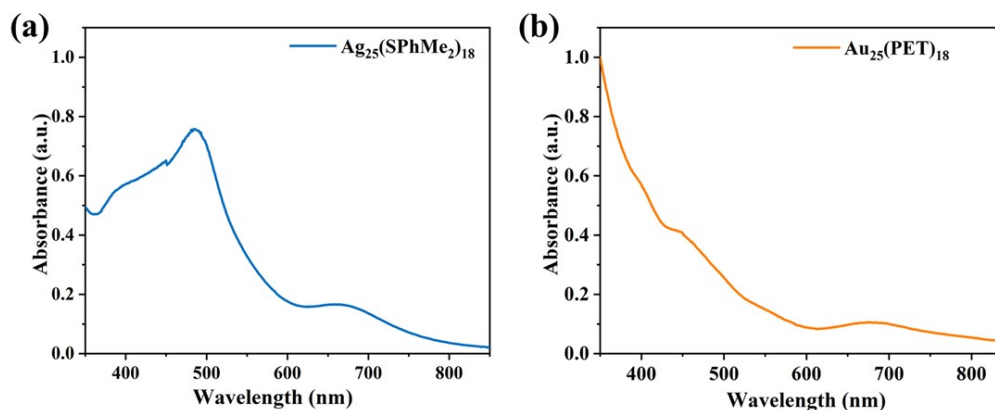
Fig.S12 UV-vis spectra of (a) $Ag_{25}(SPhMe_2)_{18}$ and (b) $Au_{25}(PET)_{18}$.

Table S1. Bader charge analysis on Ag atom in Ag_{25} at -1.10V and Au atom in Au_{25} at -0.60V based on the AIMD simulations. Blue and green highlight the Bader charge of dethiolated Ag and Au atoms, respectively.

Atom	pH=7, -1.10V	Atom	pH=7, -0.60V
Ag^1	-0.04	Au^{265}	0.00
Ag^2	0.09	Au^{266}	0.03
Ag^3	0.09	Au^{267}	0.05
Ag^4	0.10	Au^{268}	0.05
Ag^5	0.10	Au^{269}	0.04
Ag^6	0.12	Au^{270}	0.07
Ag^7	0.11	Au^{271}	0.07
Ag^8	0.10	Au^{272}	0.06
Ag^9	0.13	Au^{273}	-0.13
Ag^{10}	0.12	Au^{274}	0.04
Ag^{11}	0.11	Au^{275}	0.08

Ag^{12}	0.10	Au^{276}	0.08
Ag^{13}	0.10	Au^{277}	0.01
Ag^{14}	0.29	Au^{278}	0.04
Ag^{15}	0.29	Au^{279}	0.05
Ag^{16}	0.06	Au^{280}	-0.09
Ag^{17}	0.25	Au^{281}	0.03
Ag^{18}	0.30	Au^{282}	0.04
Ag^{19}	0.27	Au^{283}	0.08
Ag^{20}	0.03	Au^{284}	0.12
Ag^{21}	0.28	Au^{285}	0.08
Ag^{22}	0.24	Au^{286}	0.05
Ag^{23}	0.28	Au^{287}	0.07
Ag^{24}	0.25	Au^{288}	0.07
Ag^{25}	0.25	Au^{289}	-0.05

References

1   H. Cao, Z. Zhang, J.-W. Chen and Y.-G. Wang, ACS Catal., 2022, **12**, 6606-6617.

2   J. VandeVondele, M. Krack, F. Mohamed, M. Parrinello, T. Chassaing and J. Hutter, Comput. Phys. Commun., 2005, **167**, 103-128.

3   J. P. Perdew, K. Burke and M. Ernzerhof, Phys. Rev. Lett., 1996, **77**, 3865.

4   W. G. Hoover, Phys. Rev. A , 1985, **31**, 1695.

5   G. J. Martyna, M. L. Klein and M. Tuckerman, J. Chem. Phys., 1992, **97**, 2635-2643.

6   K. Xie, F. Wang, F. Wei, J. Zhao and S. Lin, J. Phys. Chem. C , 2022, **126**, 5180-5188.

7   M. Zhu, W. T. Eckenhoff, T. Pintauer and R. Jin, J. Phys. Chem. C, 2008, **112**, 14221–14224.

8   X. Liu, J. Yuan, C. Yao, J. Chen, L. Li, X. Bao, J. Yang and Z. Wu, J. Phys. Chem. C, 2017, **121**, 13848-13853.